β-decay properties of neutron-rich Zr and Mo isotopes

P. Sarriguren[1,*] and J. Pereira[2]

[1]*Instituto de Estructura de la Materia, CSIC, Serrano 123, E-28006 Madrid, Spain*

[2]*National Superconducting Cyclotron Laboratory, Michigan State University, East Lansing, Michigan 48823, USA*

(Received 2 March 2010; revised manuscript received 21 April 2010; published 18 June 2010)

Gamow-Teller strength distributions, β-decay half-lives, and β-delayed neutron emission are investigated in neutron-rich Zr and Mo isotopes within a deformed quasiparticle random-phase approximation. The approach is based on a self-consistent Skyrme Hartree-Fock mean field with pairing correlations and residual separable particle-hole and particle-particle forces. Comparison with recent measurements of half-lives stresses the important role that nuclear deformation plays in the description of β-decay properties in this mass region.

DOI: 10.1103/PhysRevC.81.064314 PACS number(s): 23.40.Hc, 21.60.Jz, 27.60.+j, 26.30.−k

I. INTRODUCTION

The rapid neutron-capture process (r process) is considered to be the main nucleosynthesis mechanism responsible for the production of heavy neutron-rich nuclei and for the existence of about half of the nuclei heavier than iron [1,2]. Although the astrophysical sites for this process are still controversial, it takes place in scenarios characterized by very high neutron densities. The path that nucleosynthesis follows involves neutron-rich isotopes, which can be far away from the valley of β stability. The most relevant nuclear properties to describe the r process are the nuclear masses and the β-decay properties [2,3]—namely, the β-decay half-lives ($T_{1/2}$) and the β-delayed neutron-emission probabilities (P_n). Nuclear masses define the possible r-process paths near the neutron drip lines. The $T_{1/2}$ values of r-process waiting-point nuclei determine the pre-freeze-out isotopic abundances and the speed of the process toward heavier elements, as well as the r-process time scale. The P_n values of r-process isobaric nuclei define the decay path toward stability following the freeze-out and provide a source of late-time neutrons.

A reliable nuclear physics description of the properties of the extremely neutron-rich nuclei along the r-process path is needed to interpret the astrophysical observations and to model and simulate the r process properly. The quality of nucleosynthesis modeling is directly affected by the quality of the nuclear structure input. Unfortunately, most of the nuclear properties of relevance for the r process are experimentally unknown, although much effort has been focused on this recently, and therefore theoretical predictions must be considered. Such calculations are particularly challenging in the very exotic regions of interest, as they involve extrapolations using well-established nuclear-structure models that have been properly tuned to account mostly for the properties of nuclei in the valley of stability. In particular, the shell structure of neutron-rich drip-line nuclei is still unknown to a large extent. Significant isospin dependence of shell effects in medium-mass and heavy nuclei has been predicted [4–6]. It has been found that the shell gaps decrease dramatically near the neutron drip lines because of continuum effects, and a quenching of shell effects is apparent.

As a matter of fact, nuclear structure properties of nuclei far from stability, where no experiments exist for direct comparison, can be tested by exploring their influence on the solar r-process abundance patterns. For example, the agreement with the observed r-process abundances in the $A \sim 120$ mass region is manifestly improved [7–10] when using nuclear structure models that include a shell quenching effect at $N = 82$ [5,11].

In this work we focus our attention on the mass region of neutron-rich $A \sim 100$–110 nuclei, which is of great interest for the astrophysical r process. In addition, neutron-rich isotopes in this mass region are known [12] to be interesting examples where the equilibrium shape of the nucleus is rapidly changing and shape coexistence is present, with competing prolate, oblate, and spherical shapes at close energies (see, e.g., Ref. [13] for a general review).

In a recent publication [14], the β-decay properties of some neutron-rich Zr and Mo isotopes were measured for the first time. The data were interpreted in terms of the quasiparticle random-phase approximation (QRPA) [15–18], using nuclear shapes and nuclear masses derived from the finite-range droplet model (FRDM) [19] and the latest version of the finite-range liquid-drop model (FRLDM) [20], which also includes triaxial deformation. QRPA calculations for neutron-rich nuclei have also been performed within different approaches, such as the Hartree-Fock-Bogoliubov (HFB) [21], the continuum QRPA, either with the extended Thomas-Fermi plus Strutinsky integral (ETFSI) method [22] or based on density functionals [23,24], and the relativistic mean-field (RMF) approach [25], to mention just some of the recent publications, all of them for spherical nuclei. However, the mass region of concern here requires nuclear deformation as a relevant degree of freedom to characterize the nuclear structure involved in the calculation of the β-strength functions. The deformed QRPA formalism has been developed in Refs. [15–17] and [26–28], where phenomenological mean fields based on Nilsson or Woods-Saxon potentials were used as a starting basis. In this work we investigate the decay properties of neutron-rich even-even Zr and Mo isotopes within a deformed self-consistent Hartree-Fock (HF) mean-field formalism with Skyrme interactions and pairing correlations in the BCS

*sarriguren@iem.cfmac.csic.es

 ©2010 The American Physical Society

approximation. Residual spin-isospin interactions are also included in the particle-hole and particle-particle channels and are treated in QRPA [29,30].

The paper is organized as follows. In Sec. II a brief review of the theoretical formalism is presented. Sec. III contains the results obtained within this approach for the potential energy curves, Gamow-Teller (GT) strength distributions, and β-decay half-lives. Section IV summarizes the main conclusions.

II. THEORETICAL FORMALISM

In this section we show briefly the theoretical framework used in this paper to describe the β-decay properties of Zr and Mo neutron-rich isotopes. More details of the formalism are given in Refs. [29] and [30]. The method consists of a self-consistent formalism based on a deformed Hartree-Fock mean field obtained with Skyrme interactions, including pairing correlations. The single-particle energies, wave functions, and occupation probabilities are generated from this mean field. In this work we have chosen the Skyrme force SLy4 [31] as a representative of the Skyrme forces. This particular force includes some selected properties of unstable nuclei in the adjusting procedure of the parameters. It is one of the more successful Skyrme forces and has been studied extensively in the last years.

The solution of the HF equation is found by using the formalism developed in Ref. [32], assuming time reversal and axial symmetry. The single-particle wave functions are expanded in terms of the eigenstates of an axially symmetric harmonic oscillator in cylindrical coordinates, using 12 major shells. The method also includes pairing between like nucleons in the BCS approximation with fixed gap parameters for protons and neutrons, which are determined phenomenologically from the odd-even mass differences through a symmetric five-term formula involving the experimental binding energies [33] when available. In those cases where experimental information for masses is still not available, we have used the same pairing gaps as for the closer isotopes measured. The pairing gaps for protons (Δ_p) and neutrons (Δ_n) obtained in this way are roughly 1 MeV. The corresponding pairing strengths G_p and G_n calculated from the gap equation depend sensitively on the mass region, single-particle spectrum, and active window for pairing. For typical values of the cutoffs of about 5 MeV around the Fermi level, one obtains $G_p \sim 0.25$ MeV and $G_n \sim 0.30$ MeV. It is worth noting that, although the BCS formalism leads to an unphysical neutron gas surrounding the nucleus near the drip line, the approximation is still valid in the region considered here, where the pairing gaps are still much lower than the Fermi energies.

The potential energy curves are analyzed as a function of the quadrupole deformation β,

$$\beta = \sqrt{\frac{\pi}{5}}\frac{Q_0}{A\langle r^2\rangle}, \tag{1}$$

written in terms of the mass quadrupole moment Q_0 and the mean square radius $\langle r^2\rangle$. For that purpose, constrained HF calculations are performed with a quadratic constraint [34]. The HF energy is minimized under the constraint of keeping the nuclear deformation fixed. Calculations of GT strengths are performed subsequently for the equilibrium shapes of each nucleus, that is, for the solutions, in general deformed, for which minima are obtained in the energy curves. Because decays connecting different shapes are disfavored, similar shapes are assumed for the ground state of the parent nucleus and for all populated states in the daughter nucleus. The validity of this assumption is discussed, for example, in Refs. [15] and [26]. In our particular case, for SLy4 and neutron-rich Zr and Mo isotopes, the ground-state deformation of the even-even parents (Zr, Mo) and of the corresponding β-decay odd-odd daughters (Nb, Tc) are practically the same, as shown in Ref. [35].

To describe GT transitions, a spin-isospin residual interaction is added to the mean field and treated in a deformed proton-neutron QRPA [15–17,26–30]. This interaction contains two parts, particle-hole (ph) and particle-particle (pp). The interaction in the ph channel is responsible for the position and structure of the GT resonance [26,29,30], and it can be derived consistently from the same Skyrme interaction used to generate the mean field, through the second derivatives of the energy density functional with respect to the one-body densities. The residual interaction is finally expressed in a separable form by averaging the Landau-Migdal resulting force over the nuclear volume, as explained in Refs. [29] and [30]. The coupling strength is given by $\chi_{\rm GT}^{\rm ph} = 0.15$ MeV. The pp part is a neutron-proton pairing force in the $J^\pi = 1^+$ coupling channel, which is also introduced as a separable force [27,28]. The strength of the pp residual interaction in this theoretical approach is not derived self-consistently from the SLy4 force used to obtain the mean field basis, but nevertheless, it has been fixed in accordance with it. This strength is usually fitted to reproduce globally the experimental half-lives. Various attempts have been made in the past to fix this strength, arriving at expressions such as $\kappa_{\rm GT}^{\rm pp} = 0.58/A^{0.7}$ in Ref. [26], which depend on the model used to describe the mean field, the Nilsson model in the reference cited. Our work in the past (see Refs. [36] and [37] and references therein), based on the Skyrme force SLy4, leads us to consider the value $\kappa_{\rm GT}^{\rm pp} = 0.03$ MeV as a reasonable choice in this mass region, improving the agreement with the experimental half-lives.

The proton-neutron QRPA phonon operator for GT excitations in even-even nuclei is written as

$$\Gamma^+_{\omega_K} = \sum_{\pi\nu}\left[X^{\omega_K}_{\pi\nu}\alpha^+_\nu\alpha^+_{\bar\pi} + Y^{\omega_K}_{\pi\nu}\alpha_{\bar\nu}\alpha_\pi\right], \tag{2}$$

where $\alpha^+(\alpha)$ are quasiparticle creation (annihilation) operators, ω_K are the QRPA excitation energies with respect to the ground state of the parent nucleus, and $X^{\omega_K}_{\pi\nu}$ and $Y^{\omega_K}_{\pi\nu}$ are the forward and backward amplitudes, respectively. For even-even nuclei the allowed GT transition amplitudes in the intrinsic frame connecting the QRPA ground state $|0\rangle$ ($\Gamma_{\omega_K}|0\rangle = 0$) to one-phonon states $|\omega_K\rangle$ ($\Gamma^+_{\omega_K}|0\rangle = |\omega_K\rangle$) are given by

$$\langle\omega_K|\sigma_K t^\pm|0\rangle = \mp M^{\omega_K}_\pm, \tag{3}$$

where

$$M_{-}^{\omega_K} = \sum_{\pi\nu} \left(q_{\pi\nu} X_{\pi\nu}^{\omega_K} + \tilde{q}_{\pi\nu} Y_{\pi\nu}^{\omega_K} \right), \quad (4)$$

$$M_{+}^{\omega_K} = \sum_{\pi\nu} \left(\tilde{q}_{\pi\nu} X_{\pi\nu}^{\omega_K} + q_{\pi\nu} Y_{\pi\nu}^{\omega_K} \right), \quad (5)$$

with

$$\tilde{q}_{\pi\nu} = u_\nu v_\pi \sum_K^{\nu\pi}, \quad q_{\pi\nu} = v_\nu u_\pi \sum_K^{\nu\pi}, \quad (6)$$

v's the occupation amplitudes ($u^2 = 1 - v^2$) and $\Sigma_K^{\nu\pi}$ the spin matrix elements connecting neutron and proton states with spin operators,

$$\sum_K^{\nu\pi} = \langle \nu | \sigma_K | \pi \rangle. \quad (7)$$

The GT strength $B_\omega(\mathrm{GT}^\pm)$ in the laboratory system for a transition $I_i K_i(0^+0) \rightarrow I_f K_f(1^+K)$ can be obtained in terms of the intrinsic amplitudes in Eq. (3) as

$$B_\omega(\mathrm{GT}^\pm) = \sum_{\omega_K} [\langle \omega_{K=0} | \sigma_0 t^\pm | 0 \rangle^2 \delta(\omega_{K=0} - \omega) + 2 \langle \omega_{K=1} | \sigma_1 t^\pm | 0 \rangle^2 \delta(\omega_{K=1} - \omega)], \quad (8)$$

in units of $g_A^2/4\pi$. To obtain this expression, the initial and final states in the laboratory frame have been expressed in terms of the intrinsic states using the Bohr-Mottelson factorization [38].

The excitation energy E_{ex} referred to the ground state of the odd-odd daughter nucleus is obtained by subtracting the lowest two-quasiparticle energy E_0 from the calculated ω energy in the QRPA calculation, $E_{\mathrm{ex}} = \omega_{\mathrm{QRPA}} - E_0$, where $E_0 = (E_n + E_p)_0$ is the sum of the lowest quasiparticle energies for neutrons and protons. The GT strength $B(\mathrm{GT})$ will be plotted later versus E_{ex} in Figs. 3–6.

The β-decay half-life is obtained by summing all the allowed transition strengths to states in the daughter nucleus with excitation energies lying below the corresponding Q energy and weighted with the phase-space factors $f(Z, Q_\beta - E_{\mathrm{ex}})$,

$$T_{1/2}^{-1} = \frac{(g_A/g_V)_{\mathrm{eff}}^2}{D} \sum_{0<E_{\mathrm{ex}}<Q_\beta} f(Z, Q_\beta - E_{\mathrm{ex}}) B(\mathrm{GT}, E_{\mathrm{ex}}), \quad (9)$$

with $D = 6200$ s and $(g_A/g_V)_{\mathrm{eff}} = 0.77 (g_A/g_V)_{\mathrm{free}}$, where 0.77 is a standard quenching factor that takes into account in an effective way all the correlations [39] tha are not properly considered in the present approach. The bare results can be recovered by scaling the results in this paper for $B(\mathrm{GT})$ and $T_{1/2}$ with the square of this quenching factor. The Q_{β^-} energy is given by

$$Q_{\beta^-} = M(A, Z) - M(A, Z+1) - m_e = \mathrm{BE}(A, Z) - \mathrm{BE}(A, Z+1) + m_n - m_p - m_e, \quad (10)$$

written in terms of the nuclear masses $M(A, Z)$ or nuclear binding energies $\mathrm{BE}(A, Z)$ and the neutron (m_n), proton (m_p), and electron (m_e) masses.

The Fermi integral $f(Z, Q_\beta - E_{\mathrm{ex}})$ is computed numerically for each value of the energy including screening and finite-size effects, as explained in Ref. [40]:

$$f^{\beta^\pm}(Z, W_0) = \int_1^{W_0} pW(W_0 - W)^2 \lambda^\pm(Z, W) \mathrm{d}W, \quad (11)$$

with

$$\lambda^\pm(Z, W) = 2(1+\gamma)(2pR)^{-2(1-\gamma)} e^{\mp \pi y} \frac{|\Gamma(\gamma + iy)|^2}{[\Gamma(2\gamma+1)]^2}, \quad (12)$$

where $\gamma = \sqrt{1 - (\alpha Z)^2}$, $y = \alpha ZW/p$, α is the fine structure constant, and R the nuclear radius. W is the total energy of the β particle, W_0 is the total energy available in $m_e c^2$ units, and $p = \sqrt{W^2 - 1}$ is the momentum in $m_e c$ units.

This function weights the strength $B(\mathrm{GT})$ differently depending on the excitation energy. As a general rule, $f(Z, Q_\beta - E_{\mathrm{ex}})$ increases with the energy of the β particle and therefore the strengths located at low excitation energies contribute more importantly to the half-life.

The probability of β-delayed neutron emission is given by

$$P_n = \frac{\sum_{S_n<E_{\mathrm{ex}}<Q_\beta} f(Z, Q_\beta - E_{\mathrm{ex}}) B(\mathrm{GT}, E_{\mathrm{ex}})}{\sum_{0<E_{\mathrm{ex}}<Q_\beta} f(Z, Q_\beta - E_{\mathrm{ex}}) B(\mathrm{GT}, E_{\mathrm{ex}})}, \quad (13)$$

where the sums extend to all the excitation energies in the daughter nuclei in the indicated ranges. S_n is the one-neutron separation energy in the daughter nucleus. In this expression it is assumed that all the decays to energies above S_n in the daughter nuclei always lead to delayed neutron emission, and then γ decay from neutron unbound levels is neglected. According to Eq. (13), P_n is mostly sensitive to the strength located at energies around S_n, thus providing a structure probe complementary to $T_{1/2}$.

III. RESULTS

In this section we start by showing the results obtained for the potential energy curves in the isotopes under study. Then we calculate the energy distribution of the GT strength corresponding to the local minima in the potential energy curves. After showing the predictions of various mass models for the Q_β and S_n values for more unstable isotopes, where no data on these quantities are available, we calculate the β-decay half-lives and discuss their dependence on the deformation.

In previous works [29,30,41–44] we have studied the sensitivity of the GT strength distributions to the various ingredients contributing to the deformed QRPA-like calculations, namely, to the nucleon-nucleon effective force, to pairing correlations, and to residual interactions. We found different sensitivities to them. In this work, all of these ingredients have been fixed to the most reasonable choices found previously and already mentioned, including the quenching factor. Here, we mainly discuss effects of deformation, keeping in mind that the method provides the self-consistent deformations as well.

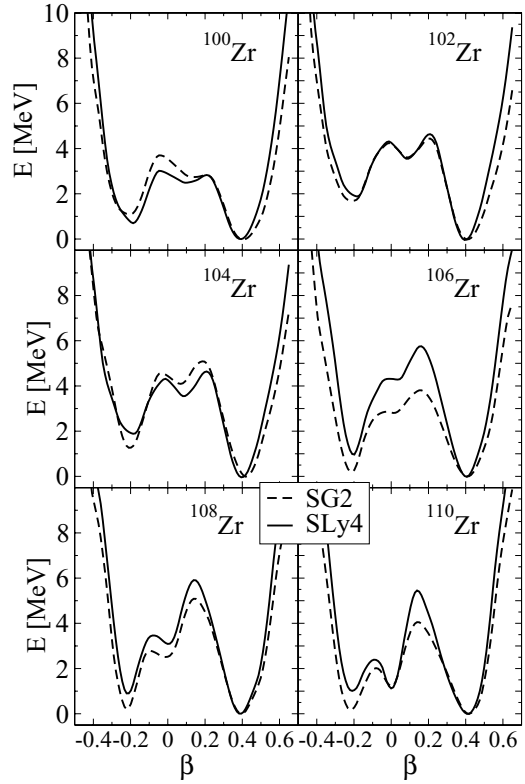

FIG. 1. Potential energy curves for even-even $^{100-110}$Zr isotopes obtained from constrained HF + BCS calculations with the Skyrme forces SG2 and SLy4.

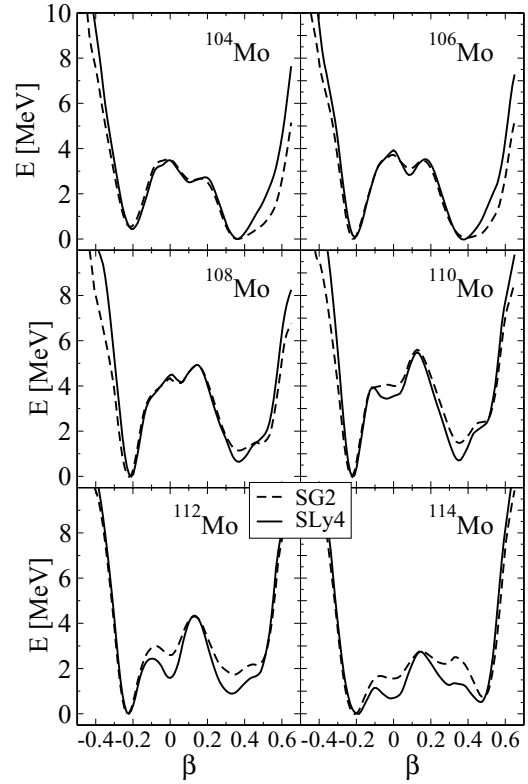

FIG. 2. Same as Fig. 1, but for $^{104-114}$Mo isotopes.

A. Potential energy curves

Figures 1 and 2 show the potential energy curves for the even-even $^{100-110}$Zr and $^{104-114}$Mo isotopes, respectively. The energies are shown relative to that of the ground state plotted as a function of the quadrupole deformation β. They were obtained from constrained HF + BCS calculations with the Skyrme forces SG2 [45] and SLy4 [31]. We observe that both forces produce very similar results. In Fig. 1 we see that the Zr isotopes exhibit, in all cases, two well-developed minima. The ground states are located in the prolate sector at positive values of $\beta \approx 0.4$. We can also see oblate minima at higher energies located at $\beta \approx -0.2$. The two minima are separated by potential energy barriers varying from $E = 3$ MeV, in the lightest ^{100}Zr isotope, up to barriers of the order of 5 MeV, in heavier isotopes. In the $^{108-110}$Zr isotopes a spherical local minimum is also developed.

Similar trends are shown in Fig. 2 for the Mo isotopes. We observe well-developed oblate and prolate minima, which are separated by barriers ranging from 3 to 5 MeV. We get a prolate ground state with an oblate minimum very close in energy to the lightest isotope considered, ^{104}Mo, a practically degenerate oblate-prolate in ^{106}Mo, and oblate ground states in heavier isotopes with quadrupole deformations at $\beta \approx -0.2$ with prolate excited states at energies lower than 1 MeV. Again, the heavier isotopes favor the appearance of a spherical configuration at very low energies, resulting in an emergent triple oblate-spherical-prolate shape coexistence scenario.

These results are in qualitative agreement with similar ones obtained in this mass region from different theoretical approaches. As an example of these methods we can mention the results obtained in Ref. [46], where this mass region was studied within a macroscopic-microscopic approach based on an energy obtained from a liquid drop or an FRLDM modified by a shell correction taken from a deformed Woods-Saxon potential. Zr isotopes from $N = 60$ to $N = 72$ were predicted to have well-deformed prolate ground states, while Mo isotopes suffered a shape transition from prolate shapes in the lighter neutron-rich isotopes ($N = 62$) to oblate shapes in the heavier ones. Similarly, the deformations obtained in Ref. [19] from the FRDM and a folded-Yukawa single-particle microscopic model were in the range $\beta = 0.36$–0.38 in the Zr isotopes considered in this work and $\beta = 0.33$–0.36 in the Mo isotopes, except in the heavier ^{114}Mo, where an oblate shape with $\beta \approx -0.25$ becomes the ground state. RMF calculations [47,48] show ground-state deformations in the range of $\beta = 0.36$–0.40 in the Zr isotopes, while for Mo isotopes oblate ground states are obtained, with parameters of deformation between $\beta = -0.28$ and $\beta = -0.23$, except in the lighter isotope ^{104}Mo, where a prolate ground state $\beta = 0.336$ is found. Calculations including rotational states in terms of the total Routhian surface, using nonaxial Wood-Saxon potentials [49], predicted two coexisting prolate and oblate minima ($\beta \approx 0.35$ and $\beta \approx -0.2$) for $^{106-116}$Zr isotopes, where the prolate ground state becomes oblate beyond ^{110}Zr. The same calculations showed oblate ($\beta \approx -0.22$) ground states for $N > 68$ Mo isotopes. Finally, similar results in the sense of competing oblate and prolate shapes and emergence

of spherical configurations in the heavier isotopes are also obtained within the HFB framework with the finite-range effective Gogny interaction D1S [50]. Equilibrium oblate ($\beta \approx -0.2$) and prolate ($\beta \approx 0.4$) coexistent deformations were found in Ref. [50] at practically the same energy in the Zr isotopes. In Mo isotopes an oblate shape ($\beta \approx -0.2$) is favored energetically with close prolate ($\beta \approx 0.4$) solutions. In both cases, Zr and Mo isotopes, a spherical solution decreases in energy and becomes almost degenerate with the deformed solutions for the heavier isotopes ^{110}Zr and ^{114}Mo.

Thus, a consistent theoretical picture emerges, which is supported by the still scarce experimental information available. Experimentally, two coexisting deformed bands weakly admixed were found in ^{100}Zr [51,52] from an analysis of $B(E2)$ and $\rho(E0)$ and a two-level mixing model analysis. One of these bands is a highly deformed prolate yrast band ($\beta = 0.34$), while the other is moderately deformed ($|\beta| = 0.16$) and weakly mixed with the yrast, by about 10%. The highly deformed band in ^{100}Zr is nearly identical to the yrast band in ^{102}Zr. Hill *et al.* [53] have also discussed the possibility that the 0_2^+ level measured for ^{102}Zr at 895 keV could be the head of a band with $|\beta| \approx 0.2$, similar to the S band of ^{100}Zr.

Quadrupole moments were also determined [54] for rotational bands in $^{98-104}$Zr isotopes and deformation parameters were deduced, increasing gradually from $\beta = 0.1$ at $N = 56$ up to $\beta = 0.4$ at $N = 64$. More recently [55], large deformations [$\beta = 0.47(7)$] were extracted in ^{104}Zr and in ^{106}Mo [$\beta = 0.36(7)$] from the half-lives of their 2^+ states. Spectroscopic studies of high-spin states of $^{100-104}$Zr and $^{102-108}$Mo have also been performed by Hua *et al.* [56] within the particle-rotor model. According to those authors, the difference in signature splitting observed for the $5/2^-[532]$ band between the odd Zr and the odd Mo isotopes could be attributed to the appearance of triaxiality in Mo isotopes. As already mentioned, the formalism employed in the present study does not include nonaxial deformation. This limitation, however, has no significant impact on the results discussed here. For example, the inclusion of triaxiality in the last version of the FRLDM [20] resulted in a small reduction in the ^{106,108}Mo ground-state energies (of about 250 keV) at $\gamma = 17.5^\circ$, with respect to pure prolate shapes. Similarly, Xu *et al.* [49] predicted a γ-soft triaxial minimum for ^{108}Mo.

B. Gamow-Teller strength distributions

In Figs. 3 and 4, we show the results obtained for the energy distributions of the GT strength corresponding to the oblate-prolate-spherical equilibrium shapes for which we obtained minima in the potential energy curves in Figs. 1 and 2. The results were obtained with the force SLy4, using constant pairing gaps extracted from the experimental masses (or systematics) and with residual interactions with the parameters written in Sec. II. The GT strength, in $g_A^2/4\pi$ units, is plotted versus the excitation energy of the daughter nucleus and a quenching factor 0.77 has been included.

Figures 3 and 4 contain the results for Zr and Mo isotopes, respectively. We show the energy distributions of the

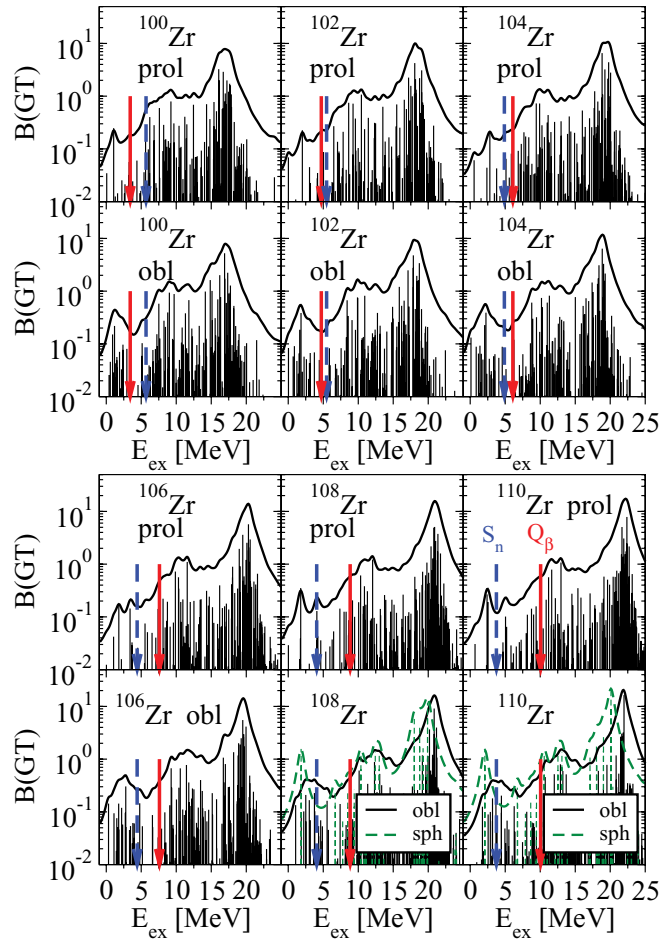

FIG. 3. (Color online) QRPA-SLy4 Gamow-Teller strength distributions for Zr isotopes as a function of the excitation energy in the daughter nucleus. Calculations correspond to the various equilibrium configurations found in the potential energy curves. Q_β and S_n values are shown by solid and dashed vertical arrows, respectively.

individual GT strengths together with continuous distributions obtained by folding the strength with 1-MeV-wide Breit-Wigner functions. The vertical arrows show the Q_β and S_n energies, taken from experiment [33] or from the mass formula in Ref. [57] when data were not available, as we explain later.

The main characteristic of these distributions is the existence of a GT resonance located at increasing excitation energy as the number of neutrons N increases. The total GT strength also increases with N, as it is expected to fulfill the Ikeda sum rule. It is worth noting that both oblate and prolate shapes produce quite similar GT strength distributions on a global scale. Even the spherical profiles are quite close to the deformed ones. Nevertheless, the small differences among the various shapes at the low-energy tails (below Q_β) of the GT strength distributions, which can be appreciated because of the logarithmic scale, lead to sizable effects in the β-decay half-lives. In Fig. 5 for Zr isotopes and Fig. 6 for Mo isotopes, we can see the accumulated GT strength plotted up to the corresponding Q_β energy of each isotope, which is the relevant energy range for calculation of the

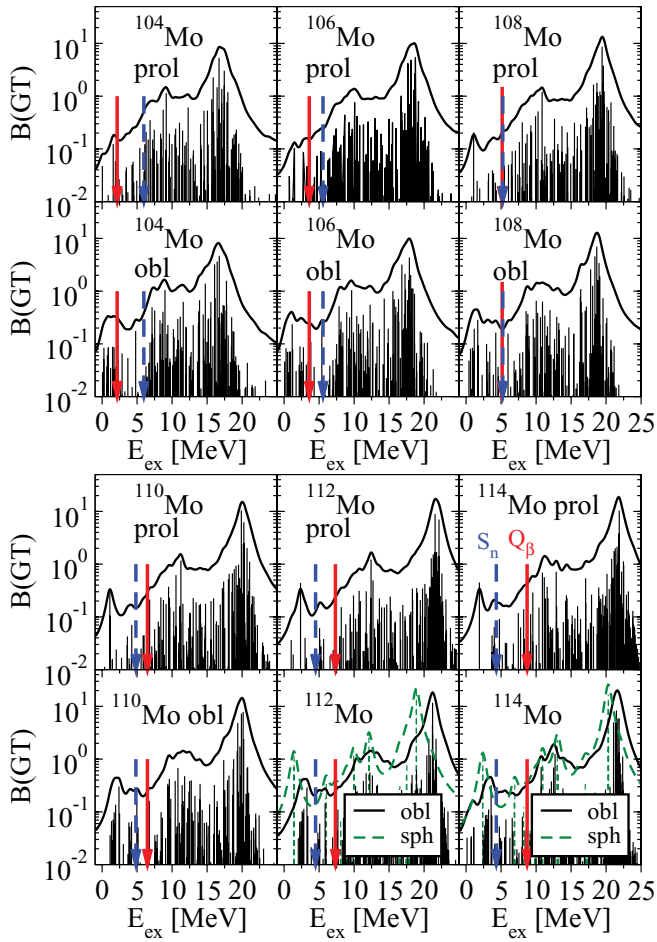

FIG. 4. (Color online) Same as Fig. 3, but for Mo isotopes.

half-lives. Also shown, by vertical dashed lines, are the S_n energies when they are lower than Q_β. At this magnified scale, one can appreciate the sensitivity of these distributions to deformation and how measurements of the GT strength distribution from β decay can be a tool to get information about this deformation, as carried out in Refs. [58] and [59]. The accumulated strength from the oblate shapes is in general larger than the corresponding prolate profiles. The spherical distributions have distinct characteristics, always appearing as a strong peak at an excitation energy of about 2 MeV. The profiles from different shapes could be easily distinguished experimentally. This is especially true in the case of the lighter isotopes $^{100-104}$Zr and $^{104-108}$Mo, where the differences are enhanced. These isotopes are, in principle, easier to measure, as they are the less exotic.

Experimental information on GT strength distributions in these isotopes is available only in the energy range below 1 MeV for the isotopes ^{106,108}Mo [60], ^{110}Mo [61], and ^{100,102,104}Zr [62]. These data are shown in Figs. 5 and 6, together with the QRPA calculations. Unfortunately, the energy region is still very narrow and represents only a small fraction of the GT strength relevant for the half-life determination. Clearly, more experimental information is needed to gain insight into the nuclear structure of these isotopes.

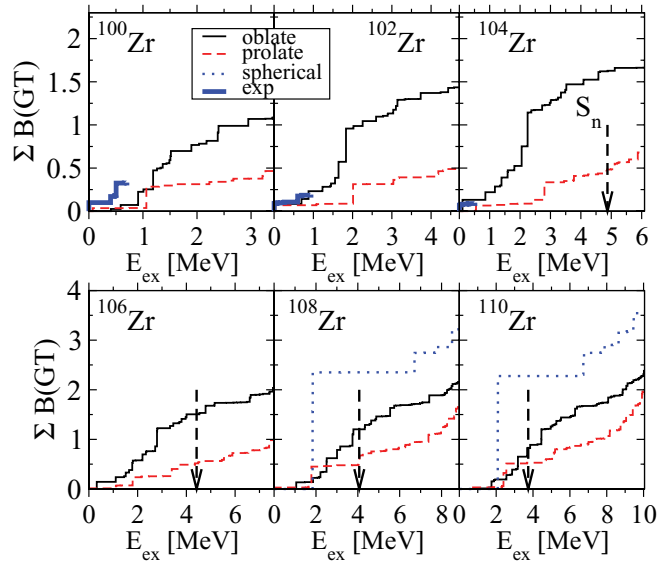

FIG. 5. (Color online) QRPA-SLy4 accumulated GT strengths in Zr isotopes calculated for the various equilibrium shapes. In each isotope the energy range considered corresponds to its Q_β value. S_n values are shown by dashed vertical arrows.

C. Half-lives and β-delayed neutron-emission probabilities

The calculation of the half-lives in Eq. (9) involves knowledge of the GT strength distribution and of the Q_β values. Calculation of the probability of β-delayed neutron emission P_n in Eq. (13) also involves knowledge of the S_n energies. We use experimental values for Q_β and S_n, which are taken from Ref. [33] or from the Jyväskylä mass database [63], when available. But in those cases where experimental masses are not available, one has to rely on theoretical predictions for them. There are a large number of mass formulas on the market, obtained from different approaches.

The strategy used in this work is, first, to compare with experiment the predictions of some representative mass formulas

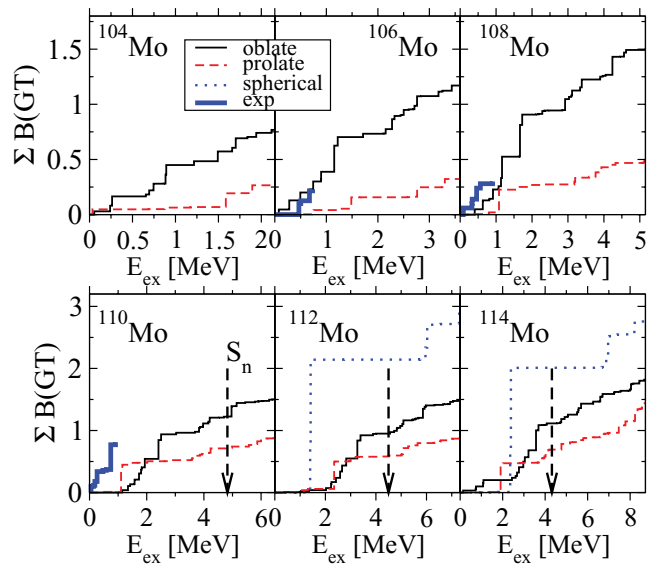

FIG. 6. (Color online) Same as Fig. 5, but for Mo isotopes.

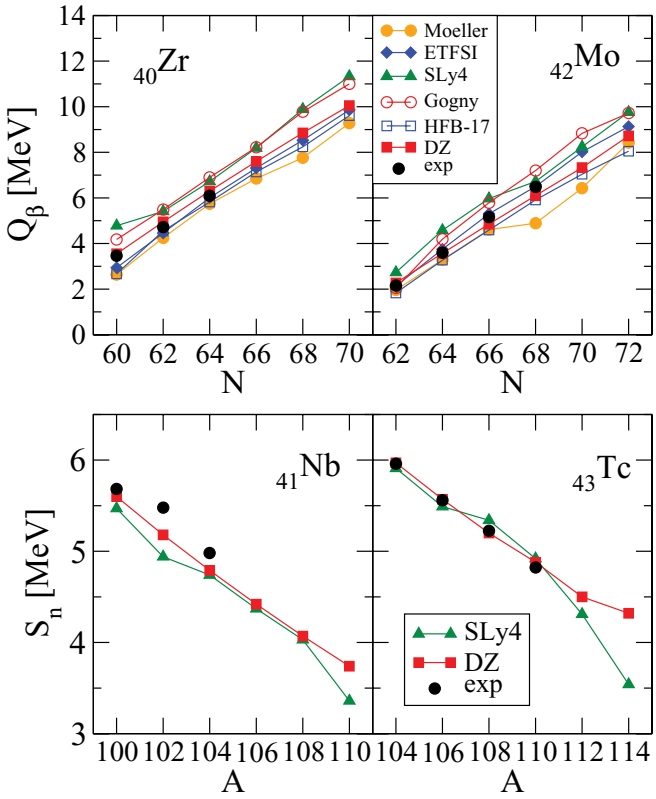

FIG. 7. (Color online) Experimental Q_β and S_n energies compared to the predictions of various mass models.

in the mass region where data are available. According to their success in reproducing the Q_β and S_n energies, we finally adopt the most convenient mass formula for extrapolations to the unknown regions.

In Fig. 7 we show this comparison for six frequently used mass formulas. We use the model of P. Möller *et al.* [19], which belongs to a microscopic-macroscopic type of calculation. It contains an FRDM corrected by microscopic effects obtained from a deformed single-particle model based on a folded Yukawa potential including pairing in the Lipkin-Nogami approach. Then we use the ETFSI model [64], which adopts a semiclassical approximation to the HF method including full Strutinsky shell corrections and BCS pairing correlations. The label SLy4 stands for the masses calculated from the Skyrme force SLy4 with a zero-range pairing force and Lipkin-Nogami obtained from the code HFBTHO [65] and compiled in Ref. [35]. The results under the label Gogny have been obtained from HFB calculations with the finite-range Gogny-D1S force [50]. The HFB-17 model is one of the most recent versions of the Skyrme HFB mass formulas introduced by the Brussels-Montreal group [66,67]. As in the previous cases, SLy4 and Gogny, this is a fully microscopic approach, as it is based on an effective two-body nucleon-nucleon interaction. The Duflo and Zuker (DZ) mass model [57] is written as an effective Hamiltonian that contains two parts, a monopole term and a multipole term. The monopole calculations are purely HF type based on single-particle properties, while the multipole term acts as a residual interaction and the calculation goes beyond HF. Its predictive power has been checked recently [68]

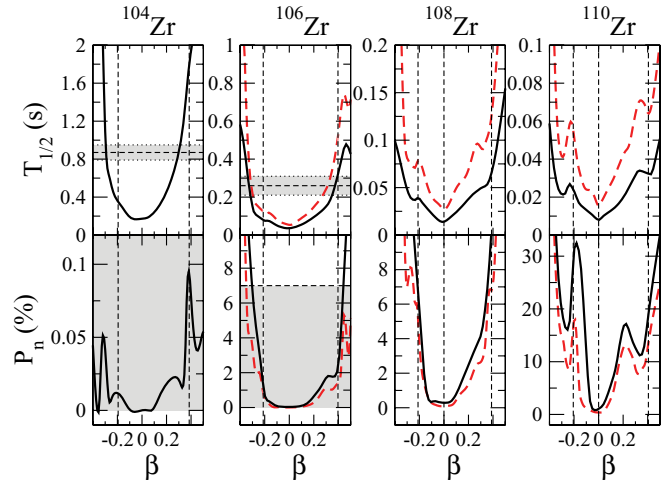

FIG. 8. (Color online) QRPA-SLy4 β-decay half-lives and P_n values for Zr isotopes as a function of the quadrupole deformation β compared to experiment (shaded area). See text for more details.

with a number of tests probing its ability to extrapolate, with very good results. In this work we use the 10-parameter version of the mass formula [69], which is a simplification of the more sophisticated 28-parameter mass formula in Ref. [57].

In the upper plots in Fig. 7 we can see the experimental Q_β values (filled circles) [33,63], available for the isotopes ^{100,102,104}Zr and ^{104,106,108,110}Mo. They are compared with the predictions of the various mass models discussed previously. The lower plots show the neutron separation energies S_n corresponding to the daughter isotopes of Nb and Tc, where we compare the measured energies (filled circles) with the predictions of the DZ formula and SLy4 force. We have selected for consistency the SLy4 predictions, but also the DZ mass formula, as one of the the most suited formulas in this particular mass region. They agree fairly well with the measured values for both Q_β and S_n values. In what follows the results for half-lives and P_n for ^{106,108,110}Zr and ^{112,114}Mo are obtained using Q_β and S_n from SLy4 and the DZ mass formula.

Figures 8 and 9 show the dependence of the half-lives $T_{1/2}$ and P_n values on the quadrupole deformation β. Solid lines in the lighter isotopes (^{104}Zr and ^{108,110}Mo) correspond to QRPA-SLy4 calculations using experimental Q_β and S_n. In the heavier isotopes ($^{106-110}$Zr and ^{112,114}Mo), where there are no data for Q_β and S_n, solid (dashed) lines correspond to QRPA-SLy4 calculations using Q_β and S_n from SLy4 (DZ). Experimental data are shown by horizontal dashed lines, and the shaded region in between corresponds to a 1-σ confidence level. The vertical dashed lines show the self-consistent quadrupole deformations for which we obtained the equilibrium shape configurations (see Figs. 1 and 2). The first evidence to mention is that a spherical approach to these nuclei is far from the measured data, demanding a deformed treatment.

In Fig. 8 we show the results for the $^{104-110}$Zr isotopes. In the cases of ^{104,106}Zr we reproduce the experimental half-lives with oblate and prolate deformations very close to the self-consistent ones. In the oblate case the calculation gives half-lives lower than experiment, while the self-consistent

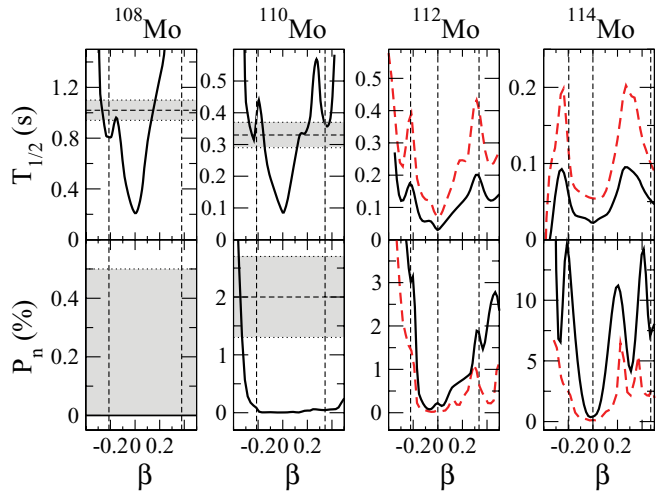

FIG. 9. (Color online) Same as Fig. 8, but for Mo isotopes.

prolate deformation produces somewhat larger ones. Thus, the experiment would be reproduced either by nuclear deformations that do not produce shapes at equilibrium ($\beta \approx \pm 0.3$) or by a mixing of the equilibrium deformations. Interestingly, similar results were obtained in Ref. [14] for ^{104}Zr, from the analysis of the measured β-decay properties of ^{104}Y in terms of quadrupole deformation ϵ_2 of the daughter ^{104}Zr (see Ref. [19] for a formal definition of the parameters ϵ_2 and β). In that case, the quadrupole deformation needed to reproduce the measured half-life and P_n value was $|\epsilon_2| \approx 0.25$, although oblate deformations were ruled out at that time. An important difference between the results shown in Fig. 8 and those discussed in Ref. [14] is the abrupt increase seen in the latter for the $T_{1/2}$ and P_n value for a near-spherical ^{104}Zr. These large values were mostly produced by the location of the GT-populated $\pi g_{9/2} \times \nu g_{7/2}$ level at rather high energies in the spherical daughter ^{104}Zr. This discrepancy emphasizes the sensitivity of $T_{1/2}$ and P_n to the structural details of the mother/daughter nuclei. The experimental P_n values are only upper limits, although they are much larger than the typical values obtained theoretically. In the heavier isotopes there are no data and these results are thus useful to see the sensitivity to deformation of the predictions. The spherical minima in the heavier isotopes predict half-lives and P_n values much lower than the corresponding values for deformed shapes. In Fig. 9 we have the results for the isotopes $^{108-114}$Mo. In the case of ^{108}Mo the half-life is reproduced with the self-consistent oblate deformation, while the prolate one generates overly high half-lives. In the case of ^{110}Mo the measured half-life is well reproduced with both oblate and prolate equilibrium deformations. In the case of ^{108}Mo the P_n value is 0, as experimentally [63] $S_n > Q_\beta$. For ^{110}Mo the P_n value is not reached by the calculations. As in the case of the heavier Zr isotopes, the heavier Mo isotopes show that the half-lives for the spherical minima are much smaller than the corresponding half-lives for the self-consistent oblate and prolate shapes. In general we observe that the half-lives (P_n values) in the heavier Zr and Mo isotopes calculated with Q_β and S_n from SLy4 (solid lines) are shorter (longer) than the results calculated with Q_β and S_n from DZ (dashed lines).

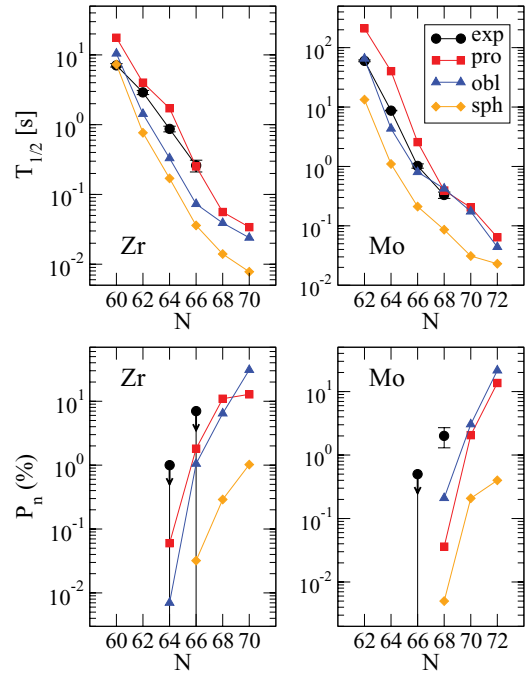

FIG. 10. (Color online) Measured β-decay half-lives and P_n values for Zr and Mo isotopes compared to theoretical QRPA results calculated from different shape configurations, using SLy4 to compute Q_β and S_n in the heavier isotopes.

In Figs. 10 and 11 we compare the measured β-decay half-lives (upper plots) and P_n values (lower plots) with the theoretical results obtained with the oblate, prolate, and spherical equilibrium shapes. In the $^{100-104}$Zr isotopes we use experimental Q_β and S_n values, while in the heavier

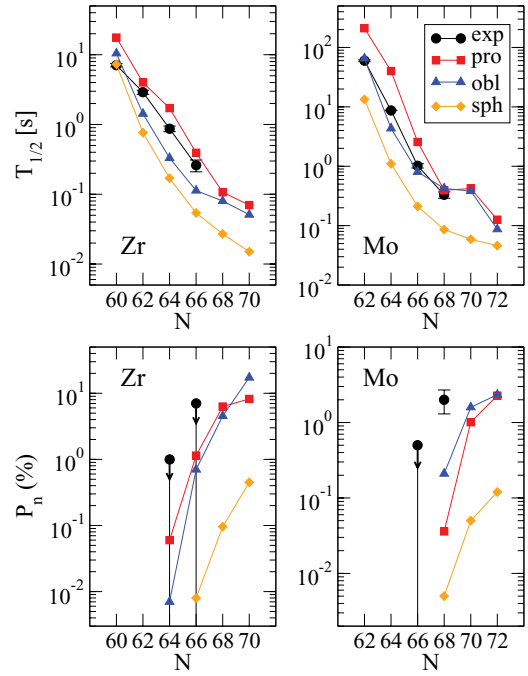

FIG. 11. (Color online) Same as Fig. 10, but using DZ instead of SLy4 to compute Q_β and S_n in the heavier isotopes.

$^{106-110}$Zr isotopes we use SLy4 in Fig. 10 and the DZ mass formula in Fig. 11. Similarly, for the $^{104-110}$Mo isotopes we use experimental Q_β and S_n values, while for $^{112-114}$Mo we use SLy4 in Fig. 10 and the DZ mass formula in Fig. 11. In the case of Zr isotopes, we can see that the experimental half-life is close to the oblate result in ^{100}Zr and it appears systematically between the prolate and the oblate calculations in the isotopes ^{102,104,106}Zr. One wonders whether this result could be explained by the coexistence of a highly deformed prolate ground-state configuration with a moderately deformed minimum similar to that found in ^{100}Zr [51,52] and (more speculatively) in ^{102}Zr [53]. The results seem to indicate that such weakly deformed intruder configurations may have an oblate character. In the heavier isotopes ^{108,110}Zr the predictions of both oblate and prolate are very close to each other and much larger than the result obtained from spherical shapes. Measurement of these half-lives and P_n values will provide a good opportunity to check the role of spherical configurations in these exotic nuclei, as the spherical components will lower the half-lives and P_n values by factors of about 5 and 15–50, respectively.

In the case of Mo isotopes, the experimental half-lives in ^{104,106,108,110}Mo tend to favor the oblate theoretical results (which are indeed the ground states) over the prolate ones. In the heavier ^{112,114}Mo isotopes, as in the case of the heavier Zr isotopes, oblate and prolate results are very similar and much larger than the spherical predictions, again offering a sensitive test to analyze the deformation of these heavy nuclei, for which spectroscopic measurements are more difficult. Experimental P_n values are only upper limits except for the case ^{110}Mo, which is much larger than the calculations. This implies that the relative GT strength contained in the energy region below S_n is overestimated theoretically, and therefore the relative contribution coming from the strength above S_n is too small. This is shown in Fig. 6 for ^{110}Mo, where the accumulated strength is practically flat above S_n. The half-lives and P_n values of the $A \sim 110$ nuclei, predicted here for spherical configurations, would have clear consequences in the calculation of r-process abundances. In particular, the abrupt reduction in the P_n values may contribute to filling the artificial trough around $A = 110$ predicted by current r-process nucleosynthesis models. Furthermore, the confirmation of spherical shapes in these nuclei may be an indirect signature of the $N = 82$ shell quenching, as both phenomena are predicted by the SLy4 force used in our calculations.

IV. CONCLUSIONS

In this paper we have studied the β-decay properties of neutron-deficient Zr and Mo isotopes within a deformed QRPA approach based on mean fields generated from self-consistent Skyrme Hartree-Fock calculations. In particular, we have analyzed the experimental information on the half-lives and β-delayed neutron-emission probabilities in the neutron-rich $^{100-110}$Zr and $^{104-114}$Mo isotopes in terms of the nuclear deformation.

We have shown that the measured half-lives in Zr isotopes are placed between the results obtained from the oblate and prolate coexistent shapes that appear to be very close in energy in the potential energy curves. The predicted half-lives for the heavier Zr isotopes ^{108,110}Zr, for which there are no experimental data yet, are, however, very close to each other for both oblate and prolate shapes and much larger than the predictions from the spherical shapes. In contrast, the measured half-lives in Mo isotopes agree better with the calculations from oblate shapes, which are lower than the corresponding prolate ones. Once more, in the heavier isotopes ^{112,114}Mo, the predicted half-lives for both shapes are very close and larger than the spherical ones. Thus, comparison with experimental half-lives indicates that in some cases (Mo isotopes) a single shape accounts for this information, while in other cases (most of the Zr isotopes) a more demanding treatment in terms of mixing of different shapes seems to be more appropriate. P_n values are in general not well reproduced, although experimentally only upper limits are measured in most cases. Hence, it will certainly be worth measuring those heavier isotopes and checking whether they are properly described by the deformed shapes or whether a spherical component is needed as well.

Nevertheless, one should keep in mind that half-lives are integral properties that collect all the information of the decay in a single number and do not tell us about the detailed internal structure of the GT strength distribution, which is much more sensitive to the nuclear structure. From a more detailed analysis of the GT strength distributions in the Q_β energy range accessible in β decay, we have shown that the differences between the predictions of the different nuclear shapes could be clearly distinguished experimentally. Although these spectroscopic measurements are not feasible at present because of the still low production rates of exotic nuclei at modern radioactive-beam facilities, they will provide precise tests of the nuclear structure in exotic nuclei in the future.

ACKNOWLEDGMENTS

This work was supported by Ministerio de Ciencia e Innovación (Spain) under Contract No. FIS2008-01301. It was also supported in part by the Joint Institute for Nuclear Astrophysics (JINA) under NSF Grant No. PHY-02-16783 and the National Superconducting Cyclotron Laboratory (NSCL) under NSF Grant No. PHY-01-10253.

[1] E. M. Burbidge, G. M. Burbidge, W. A. Fowler, and F. Hoyle, Rev. Mod. Phys. **29**, 547 (1959).
[2] J. J. Cowan, F.-K. Thielemann, and J. W. Truran, Phys. Rep. **208**, 267 (1991).
[3] K.-L. Kratz, J.-P. Bitouzet, F.-K. Thielemann, P. Möller, and B. Pfeiffer, Astrophys. J. **403**, 216 (1993).
[4] J. Dobaczewski, I. Hamamoto, W. Nazarewicz, and J. A. Sheikh, Phys. Rev. Lett. **72**, 981 (1994).

[5] J. Dobaczewski, W. Nazarewicz, T. R. Werner, J. F. Berger, C. R. Chinn, and J. Dechargé, Phys. Rev. C **53**, 2809 (1996).
[6] T. Otsuka, T. Matsuo, and D. Abe, Phys. Rev. Lett. **97**, 162501 (2006).
[7] B. Chen, J. Dobaczewski, K.-L. Kratz, K. Langanke, B. Pfeiffer, F.-K. Thielemann, and P. Vogel, Phys. Lett. B **355**, 37 (1995).
[8] B. Pfeiffer, K.-L. Kratz, and F.-K. Thielemann, Z. Phys. A **357**, 235 (1997).
[9] B. Pfeiffer, K.-L. Kratz, F.-K. Thielemann, and W. B. Walters, Nucl. Phys. A **693**, 282 (2001).
[10] B. Sun, F. Montes, L. S. Geng, H. Geissel, Yu. A. Litvinov, and J. Meng, Phys. Rev. C **78**, 025806 (2008).
[11] J. M. Pearson, R. C. Nayak, and S. Goriely, Phys. Lett. B **387**, 455 (1996).
[12] J. L. Wood, K. Heyde, W. Nazarewicz, M. Huyse, and P. Van Duppen, Phys. Rep. **215**, 101 (1992).
[13] R. F. Casten, Nucl. Phys. A **443**, 1 (1985).
[14] J. Pereira *et al.*, Phys. Rev. C **79**, 035806 (2009).
[15] J. Krumlinde and P. Möller, Nucl. Phys. A **417**, 419 (1984).
[16] P. Möller and J. Randrup, Nucl. Phys. A **514**, 1 (1990).
[17] P. Möller, J. R. Nix, and K.-L. Kratz, At. Data Nucl. Data Tables **66**, 131 (1997).
[18] P. Möller, B. Pfeiffer, and K.-L. Kratz, Phys. Rev. C **67**, 055802 (2003).
[19] P. Möller, J. R. Nix, W. D. Myers, and W. J. Swiatecki, At. Data Nucl. Data Tables **59**, 185 (1995).
[20] P. Möller, R. Bengtsson, B. G. Carlsson, P. Olivius, T. Ichikawa, H. Sagawa, and A. Iwamoto, At. Data Nucl. Data Tables **94**, 758 (2008).
[21] J. Engel, M. Bender, J. Dobaczewski, W. Nazarewicz, and R. Surman, Phys. Rev. C **60**, 014302 (1999).
[22] I. N. Borzov and S. Goriely, Phys. Rev. C **62**, 035501 (2000).
[23] I. N. Borzov, Nucl. Phys. A **777**, 645 (2007).
[24] I. N. Borzov, J. J. Cuenca-García, K. Langanke, G. Martínez-Pinedo, and F. Montes, Nucl. Phys. A **814**, 159 (2008).
[25] T. Niksic, T. Marketin, D. Vretenar, N. Paar, and P. Ring, Phys. Rev. C **71**, 014308 (2005).
[26] H. Homma, E. Bender, M. Hirsch, K. Muto, H. V. Klapdor-Kleingrothaus, and T. Oda, Phys. Rev. C **54**, 2972 (1996).
[27] M. Hirsch, A. Staudt, K. Muto, and H. V. Klapdor-Kleingrothaus, Nucl. Phys. A **535**, 62 (1991).
[28] K. Muto, E. Bender, T. Oda, and H. V. Klapdor-Kleingrothaus, Z. Phys. A **341**, 407 (1992).
[29] P. Sarriguren, E. Moya de Guerra, A. Escuderos, and A. C. Carrizo, Nucl. Phys. A **635**, 55 (1998).
[30] P. Sarriguren, E. Moya de Guerra, and A. Escuderos, Nucl. Phys. A **691**, 631 (2001).
[31] E. Chabanat, P. Bonche, P. Haensel, J. Meyer, and R. Schaeffer, Nucl. Phys. A **635**, 231 (1998).
[32] D. Vautherin and D. M. Brink, Phys. Rev. C **5**, 626 (1972); D. Vautherin, *ibid.* **7**, 296 (1973).
[33] G. Audi, O. Bersillon, J. Blachot, and A. H. Wapstra, Nucl. Phys. A **729**, 3 (2003).
[34] H. Flocard, P. Quentin, A. K. Kerman, and D. Vautherin, Nucl. Phys. A **203**, 433 (1973).
[35] [http://massexplorer.org/].
[36] P. Sarriguren, Phys. Rev. C **79**, 044315 (2009).
[37] P. Sarriguren, Phys. Lett. B **680**, 438 (2009).
[38] A. Bohr and B. Mottelson, *Nuclear Structure* (Benjamin, New York, 1975), Vol. II, p. 10.
[39] G. F. Bertsch and I. Hamamoto, Phys. Rev. C **26**, 1323 (1982).
[40] N. B. Gove and M. J. Martin, At. Data Nucl. Data Tables **10**, 205 (1971).
[41] P. Sarriguren, R. Alvarez-Rodríguez, and E. Moya de Guerra, Eur. Phys. J. A **24**, 193 (2005).
[42] P. Sarriguren, E. Moya de Guerra, and A. Escuderos, Nucl. Phys. A **658**, 13 (1999).
[43] P. Sarriguren, E. Moya de Guerra, and A. Escuderos, Phys. Rev. C **64**, 064306 (2001).
[44] P. Sarriguren, O. Moreno, R. Alvarez-Rodríguez, and E. M. de Guerra, Phys. Rev. C **72**, 054317 (2005).
[45] N. Van Giai and H. Sagawa, Phys. Lett. B **106**, 379 (1981).
[46] J. Skalski, S. Mizutori, and W. Nazarewicz, Nucl. Phys. A **617**, 282 (1997).
[47] G. A. Lalazissis and M. M. Sharma, Nucl. Phys. A **586**, 201 (1995).
[48] G. A. Lalazissis, S. Raman, and P. Ring, At. Data Nucl. Data Tables **71**, 1 (1999).
[49] F. R. Xu, P. M. Walker, and R. Wyss, Phys. Rev. C **65**, 021303(R) (2002).
[50] S. Hilaire and M. Girod, Eur. Phys. J. A **33**, 237 (2007) [http://www-phynu.cea.fr/].
[51] H. Mach *et al.*, Phys. Lett. B **230**, 21 (1989).
[52] H. Mach, M. Moszynski, R. L. Gill, G. Molnar, F. K. Wohn, J. A. Winger, and J. C. Hill, Phys. Rev. C **41**, 350 (1990).
[53] J. C. Hill, D. D. Schwellenbach, F. K. Wohn, J. A. Winger, R. L. Gill, H. Ohm, and K. Sistemich, Phys. Rev. C **43**, 2591 (1991).
[54] W. Urban *et al.*, Nucl. Phys. A **689**, 605 (2001).
[55] C. Goodin *et al.*, Nucl. Phys. A **787**, 231c (2007).
[56] H. Hua, C. Y. Wu, D. Cline, A. B. Hayes, R. Teng, R. M. Clark, P. Fallon, A. Goergen, A. O. Macchiavelli, and K. Vetter, Phys. Rev. C **69**, 014317 (2004).
[57] J. Duflo and A. P. Zuker, Phys. Rev. C **52**, R23 (1995).
[58] E. Poirier *et al.*, Phys. Rev. C **69**, 034307 (2004).
[59] E. Nácher *et al.*, Phys. Rev. Lett. **92**, 232501 (2004).
[60] A. Jokinen, T. Enqvist, P. P. Jauho, M. Leino, J. M. Parmonen, H. Penttilä, J. Äystö, and K. Eskola, Nucl. Phys. A **584**, 489 (1995).
[61] J. C. Wang *et al.*, Eur. Phys. J. A **19**, 83 (2004).
[62] S. Rinta-Antila *et al.*, Eur. Phys. J. A **31**, 1 (2007).
[63] [http://research.jyu.fi/igisol/JYFLTRAP_masses/].
[64] Y. Aboussir, J. M. Pearson, A. K. Dutta, F. Tondeur, At. Data Nucl. Data Tables **61**, 127 (1995).
[65] M. V. Stoitsov, J. Dobaczewski, W. Nazarewicz, and P. Ring, Comput. Phys. Commun. **167**, 43 (2005).
[66] S. Goriely, F. Tondeur, and J. M. Pearson, At. Data Nucl. Data Tables **77**, 311 (2001).
[67] S. Goriely, N. Chamel, and J. M. Pearson, Phys. Rev. Lett. **102**, 152503 (2009).
[68] J. Mendoza-Temis, I. Morales, J. Barea, A. Frank, J. G. Hirsch, J. C. López Vieyra, P. Van Isacker, and V. Velázquez, Nucl. Phys. A **812**, 28 (2008).
[69] J. Mendoza-Temis, J. G. Hirsch, and A. P. Zuker, Nucl. Phys. A (2010), doi:10.1016/j.nuclphysa.2010.05.055.